Physics Letters B 797 (2019) 134825

Contents lists available at ScienceDirect

Physics Letters B

www.elsevier.com/locate/physletb

Lower bound on the proton charge radius from electron scattering data

Franziska Hagelstein [a], Vladimir Pascalutsa [b,*]

[a] Albert Einstein Center for Fundamental Physics, Institute for Theoretical Physics, University of Bern, Sidlerstrasse 5, CH-3012 Bern, Switzerland
[b] Institut für Kernphysik and Cluster of Excellence PRISMA, Johannes Gutenberg Universität Mainz, D-55128 Mainz, Germany

ARTICLE INFO

Article history:
Received 1 January 2019
Received in revised form 18 July 2019
Accepted 30 July 2019
Available online 1 August 2019
Editor: V. Metag

Keywords:
Charge radius
Proton size
Form factors
Charge distribution
Electron scattering

ABSTRACT

The proton charge-radius determinations from the electromagnetic form-factor measurements in electron-proton (ep) scattering require an extrapolation to zero momentum transfer ($Q^2 = 0$) which is prone to model-dependent assumptions. We show that the data at finite momentum transfer can be used to establish a rigorous lower bound on the proton charge radius, while bypassing the model-dependent assumptions that go into the fitting and extrapolation of the ep data. The near-future precise ep experiments at very low Q^2, such as PRad, are expected to set a stringent lower bound on the proton radius.

1. Introduction

The proton charge radius is traditionally accessed in elastic electron-proton (ep) scattering at small momentum transfers (low Q) [1,2]. Recently, however, the accuracy of this method has been questioned in the context of the *proton-radius puzzle*, which is partially attributed to the discrepancy between the 2010 ep scattering value of Bernauer et al. [3,4] and the muonic-hydrogen (μH) extraction of the proton radius [5,6], see Fig. 1. Meanwhile, as seen from the figure, the different extractions based on ep-scattering data have covered a whole range of values and hardly add-up into a coherent picture.

A "weak link" of the proton-radius extractions from ep experiments is the extrapolation to zero momentum transfer. Namely, while the data taken in some finite-Q^2 range can directly be mapped into the proton (electric and magnetic) Sachs form factors $G_E(Q^2)$ and $G_M(Q^2)$, the radii extractions require the derivatives of those at $Q^2 = 0$, e.g.: $R_E = \sqrt{-6\, G'_E(0)}$. As much as one believes that the slope at 0 is largely determined by the behavior at finite Q^2, it is not easy to quantify this relation with the necessary precision. The issues of fitting and extrapolation of the form-factor data have lately been under intense discussion, see, e.g., Refs. [14, 25–27]. Similar extrapolation problems should exist in the extractions based on lattice QCD, since the lowest momentum transfer therein is severely limited by the finite volume.

Here, we show that the form-factor data at finite Q^2 provide a *lower bound* on the proton charge radius. A determination of this bound needs no extrapolation, therefore no major model assumptions, and should be based solely on experimental (or lattice) data. At the same time, given that some of the conventional extractions from ep data show a considerably larger radius than the μH value, a strict lower bound, based purely on data, is potentially useful in understanding this discrepancy.

In what follows, we briefly recall the basic formulae in Sec. 2, introduce the quantity proposed to serve as the charge-radius bound in Sec. 3, obtain an empirical value for it based on proton electric form-factor data in Sec. 4 and conclude in Sec. 5.

2. Basic ingredients of the radius extraction

Let us recall that a spin-1/2 particle, such as the proton, has two electromagnetic form factors. These are either the Dirac and Pauli form factors: $F_1(Q^2)$ and $F_2(Q^2)$; or, the electric and magnetic Sachs form factors:

$$G_E(Q^2) = F_1(Q^2) - \frac{Q^2}{4M^2} F_2(Q^2), \tag{1a}$$

$$G_M(Q^2) = F_1(Q^2) + F_2(Q^2), \tag{1b}$$

* Corresponding author.
E-mail addresses: hagelstein@itp.unibe.ch (F. Hagelstein), pascalut@uni-mainz.de (V. Pascalutsa).

https://doi.org/10.1016/j.physletb.2019.134825

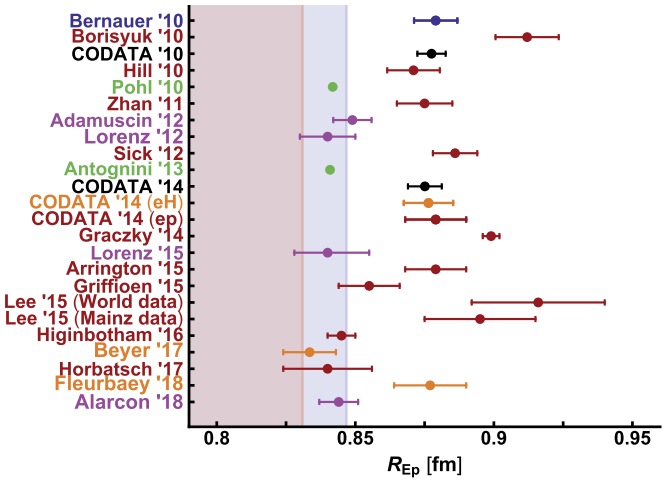

Fig. 1. Summary of different proton charge-radius extractions. A) CODATA recommended charge radii in black: '10 [7], '14 [8]. B) hydrogen and deuterium spectroscopy in orange: Beyer '17 [9], Fleurbaey '18 [10]; C) muonic-hydrogen spectroscopy in green: Pohl '10 [5], Antognini '13 [6]; D) electron-proton scattering experiments in red: Borisyuk '10 [11], Hill '10 [12] (z expansion), Zhan '11 [13] (recoil polarimetry), Sick '12 [14], Graczky '14 [15], Arrington '15 [16], Griffioen '15 [17], Lee '15 [18], Higinbotham '16 [19], Horbatsch '17 [20] (fit with chiral perturbation theory input for higher moments); E) electron-proton scattering fits within a dispersive framework in purple: Adamuscin '12 [21], Lorenz '12 [22], Lorenz '15 [23], Alarcon '18 [24]; F) electron-proton scattering data from Bernauer '10 [3] in blue. G) the bands show the "excluded region" obtained by a tentative evaluation of the lower bound from two different datasets, see Sec. 4.

with M the particle mass. The Sachs form factors can be interpreted as the Fourier transforms of the charge and magnetization distributions, $\rho_E(\vec{r})$ and $\rho_M(\vec{r})$, in the Breit frame. Strictly speaking, this relation holds only for spherically symmetric densities, in which case one has, see e.g. Ref. [28]:

$$G_E(Q^2) = 4\pi \int_0^\infty \mathrm{d}r\, r^2\, j_0(Qr)\, \rho_E(r), \tag{2a}$$

$$\frac{G_M(Q^2)}{1+\kappa} = 4\pi \int_0^\infty \mathrm{d}r\, r^2\, j_0(Qr)\, \rho_M(r), \tag{2b}$$

where $j_0(x) = \frac{\sin x}{x}$ is the spherical Bessel function, and κ is the anomalous magnetic moment of the proton. Note that these are Lorentz-invariant expressions, hence, the spherically symmetric charge and magnetization distributions are, just as the form factors, Lorentz-invariant quantities.

The radii are introduced through the density moments, which, for even k, can be given by the form-factor derivatives at 0:

$$\begin{aligned}\left\langle r^k \right\rangle_E &\equiv 4\pi \int_0^\infty \mathrm{d}r\, r^2\, r^k \rho_E(r) \\ &\overset{\text{even } k}{=} (-1)^{k/2} \frac{(k+1)!}{(k/2)!} G_E^{(k/2)}(0);\end{aligned} \tag{3}$$

and similarly for the magnetic radii with ρ_E replaced by ρ_M, and G_E replaced by $G_M/(1+\kappa)$, respectively. Therefore, the Taylor expansion of the form factor around $Q^2 = 0$ is written as:

$$\begin{aligned}G_E(Q^2) &= \sum_{n=0}^{\infty} \frac{(-1)^n}{(2n+1)!} \left\langle r^{2n} \right\rangle_E Q^{2n} \\ &= 1 - \frac{1}{6}\left\langle r^2 \right\rangle_E Q^2 + \frac{1}{120}\left\langle r^4 \right\rangle_E Q^4 + \dots\end{aligned} \tag{4}$$

The subject of interest is the root-mean-square (rms) radius (or, simply the charge radius): $R_E = \sqrt{\langle r^2 \rangle_E}$. Ideally, it could be extracted by fitting the first few terms of the above Taylor expansion of the form factor to the experimental data at low Q^2. In practice, however, this does not work. The main reason is that the convergence radius of the Taylor expansion is limited by the onset of the pion-production branch cut for time-like photon momenta at $Q^2 = -4m_\pi^2$ (the nearest singularity, as far as the strong interaction is concerned), and there are simply not many ep data for $Q^2 \ll 4m_\pi^2 \approx 0.08$ GeV^2.

A viable approach to fit to higher Q^2 is, instead of the Taylor expansion, to use a form which takes the singularities into account. This is done in the z-expansion [12] and dispersive fits [21,23, 24]. These approaches have, however, other severe limitations. The z-expansion only deals with the first singularity and therefore extends the convergence radius to $9m_\pi^2$ only. The dispersive approach is based on an exact dispersion relation for the form factor:

$$G_E(Q^2) = 1 - \frac{Q^2}{\pi} \int_{4m_\pi^2}^\infty \mathrm{d}t\, \frac{\operatorname{Im} G_E(t)}{t(t+Q^2)}, \tag{5}$$

which, in principle, accounts for all singularities. Unfortunately, it requires the knowledge of the spectral function, $\operatorname{Im} G_E(t)$, which is not directly accessible in experiment, and needs to be modeled. Chiral perturbation theory can only provide a description of this function in the range of $t \ll 1$ GeV^2. Despite the recent progress in the empirical description of the spectral function [29], the problem of model dependence of the radius extraction in the dispersive approach remains to be non-trivial.

3. Positivity bounds

Given the aforementioned issues in extracting the charge radius from form-factor data, we turn to establishing a bound on the radius, rather than the radius itself. The advantage is that the bound will follow from the finite-Q^2 data alone and needs no extrapolations or model assumptions.

To this end we consider the following quantity:

$$R_E^2(Q^2) \equiv -\frac{6}{Q^2} \ln G_E(Q^2), \tag{6}$$

which in the real-photon limit yields the radius squared:

$$\lim_{Q^2 \to 0} R_E^2(Q^2) = -6 \left. \frac{G_E'(Q^2)}{G_E(Q^2)} \right|_{Q^2=0} = R_E^2. \tag{7}$$

As will be argued in Sec. 3, the spacelike ($Q^2 \geq 0$) proton form factor is bounded from above:

$$G_E(Q^2) \leq 1, \tag{8}$$

and hence, the above log-function is positive, $R_E^2(Q^2) \geq 0$. Furthermore, if G_E falls with increasing Q^2 not faster than by a power law, then $R_E^2(Q^2)$ falls as well. The analytic properties of G_E, in the absence of zeros, are inherited by its logarithm. The subtracted dispersion relation (5) for the form factor then leads to an unsubtracted one for R_E^2:

$$R_E^2(Q^2) = \frac{1}{\pi} \int_{4m_\pi^2}^\infty \mathrm{d}t\, \frac{\operatorname{Im} R_E^2(t)}{t+Q^2}, \tag{9}$$

where $\operatorname{Im} R_E^2(t) = (6/t)\varphi_E(t)$, and $\varphi_E(t) \geq 0$ is the phase defined through $G_E(t) = |G_E(t)| e^{i\varphi_E(t)}$. This dispersion relation shows that

the function is monotonic in the spacelike region. The latter allows one to establish a *lower bound on the radius*:

$$R_E^2(Q^2) \leq R_E^2, \quad \text{for } Q^2 \geq 0. \tag{10}$$

Substituting in here the Taylor expansion, Eq. (4), one has:

$$R_E^2(Q^2) = R_E^2 - \left(\frac{1}{20}\langle r^4\rangle_E - \frac{1}{12}R_E^4\right) Q^2 + \mathcal{O}(Q^4), \tag{11}$$

and so, in order for the bound to hold at arbitrarily low Q^2, the fourth and second moments must satisfy the following inequality[1]:

$$\sqrt{\frac{3}{5}\langle r^4\rangle_E} > R_E^2. \tag{12}$$

We have checked that this non-trivial hierarchical condition on the radii, which follows from the lower bound Eq. (10), is verified in existing empirical parametrizations of the proton form factor, of which the dipole form, $G_E(Q^2) = [1 + Q^2/(0.71\,\text{GeV}^2)]^{-2}$, is the simplest one.

The fact that $R_E^2(Q^2)$ is monotonically increasing towards $Q^2 = 0$ means that the best bound is obtained at lowest accessible Q^2. In practice, however, it depends on the size of the experimental errors, including the uncertainty in the overall normalization of the form factor. We discuss this in detail in Sec. 4, when obtaining the empirical value of the bound from experimental data. In the rest of this section we focus on the proof of Eq. (8).

The unitary bound on the proton form factor, given in Eq. (8), and subsequently the radius bound, given in Eq. (10), follow from *positivity* of the corresponding charge density distribution: $\rho_E(r) \geq 0$. Indeed, from Eq. (2a),

$$G_E(0) - G_E(Q^2) = 4\pi \int_0^\infty \mathrm{d}r\, r^2 \big[1 - j_0(Qr)\big]\, \rho_E(r), \tag{13}$$

with the property of the Bessel function $j_0(x) \leq 1$, and the positivity of $\rho_E(r)$, we can see that the integrand on the right-hand side is positive definite, and Eq. (8) follows upon substituting $G_E(0) = 1$ on the left-hand side.

There is a concern [31] that the proton charge density is not necessarily positive definite, and only the transverse charge density is ($\rho_\perp(b) \geq 0$). The latter relates to the Dirac form factor through the two-dimensional Fourier transform:

$$F_1(Q^2) = 2\pi \int_0^\infty \mathrm{d}b\, b\, J_0(Qb)\, \rho_\perp(b), \tag{14}$$

where $J_0(x)$ is the cylindrical Bessel function. However, the positivity of the transverse charge density is sufficient to prove the unity bound of Eq. (8). To see this, one may apply the previous argument [cf. Eq. (13)] to Eq. (14) using $J_0(x) \leq 1$, and derive the bound on the Dirac form factor:

$$F_1(Q^2) \leq 1. \tag{15}$$

Then, the unitary bound on G_E follows from its definition in terms of the Dirac and Pauli form factors, see Eq. (1a), by taking into account the conditions $F_1(Q^2) \leq 1$ and $F_2(Q^2) \geq 0$. The latter is valid for the proton in at least the low-Q region, as can be seen empirically from $F_2(0) = \kappa$, with $\kappa \simeq 1.79$ the anomalous magnetic moment of the proton.

While the unity bound on G_E follows from the positivity of $\rho_E(r)$, the reverse is not necessarily true. Therefore, the proof based on the positivity of the transverse charge density $\rho_\perp(b)$ does not necessarily imply the positivity of $\rho_E(r)$. Introducing $\rho_1(r)$ as the three-dimensional Fourier-transform of the Dirac form factor, we have:

$$F_1(Q^2) = 4\pi \int_0^\infty \mathrm{d}r\, r^2\, j_0(Qr)\, \rho_1(r), \tag{16}$$

and matching it to Eq. (14), we obtain its relation to the transverse density[2]:

$$\rho_\perp(b) = 2\int_b^\infty \mathrm{d}r\, \frac{r}{\sqrt{r^2 - b^2}}\, \rho_1(r) \tag{17a}$$

$$= \int_{-\infty}^\infty \mathrm{d}z\, \rho_1\big(\sqrt{b^2 + z^2}\big). \tag{17b}$$

The two are thus related by the *Abel transform* [32, p. 351 et seqq.]. It infers $\rho_\perp \geq 0$, for $\rho_1 \geq 0$, while the reverse is not necessarily true.

4. Exploring the *ep* scattering data

4.1. Direct determination

We now proceed to obtaining the lower bound on the proton charge radius from *ep* scattering data. The first step is to convert the experimental data for $G_E(Q^2)$ to $R_E^2(Q^2)$, using the definition (6). The presently available data in the region well below the pion-pair production scale (here we chose $Q^2 < 0.02$ GeV^2) are shown in Fig. 2. The light-blue points are from the dataset of Bernauer et al. [3,4]. The light-red data points are from the recent initial-state radiation (ISR) experiment at MAMI [30]. In both cases we show the statistical error bars only (the systematic error will be discussed below and taken into account for Bernauer's data). The two points at $Q^2 = 0$ indicate the muonic-hydrogen (green) and Bernauer's *ep*-scattering (dark-blue) values of the proton charge radius.

In principle, every data point in Fig. 2, at finite Q^2, provides a lower bound on the proton charge radius. For a more accurate

[1] Based on Eq. (9), one can claim that $R_E^2(Q^2)$ is completely monotonic, i.e.: $(-1)^n \mathrm{d}^n R_E^2(Q^2)/\mathrm{d}(Q^2)^n \geq 0$, from which the lower bounds on other radii can be derived. The lowest values of the radii are given in terms of the charge radius R_E, and can all be obtained from Taylor-expanding the following form of the form factor: $G_E^{(\min)}(Q^2) = \exp\big(-\frac{1}{6}R_E^2 Q^2\big)$.

[2] Here we recall the following relations between the spherical and cylindrical Bessel functions:

$$J_0(x) = \frac{2}{\pi}\int_x^\infty \mathrm{d}x'\, x'\, \frac{j_0(x')}{\sqrt{x'^2 - x^2}},$$

$$j_0(x) = \frac{1}{x}\int_0^x \mathrm{d}x'\, x'\, \frac{J_0(x')}{\sqrt{x^2 - x'^2}},$$

as well as their orthogonality:

$$\int_0^\infty \mathrm{d}Q\; Q\; J_l(Qb)\, J_l(Qb') = \frac{1}{b}\delta(b - b'),$$

$$\int_0^\infty \mathrm{d}Q\; Q^2\, j_l(Qr)\, j_l(Qr') = \frac{\pi}{2r^2}\delta(r - r').$$

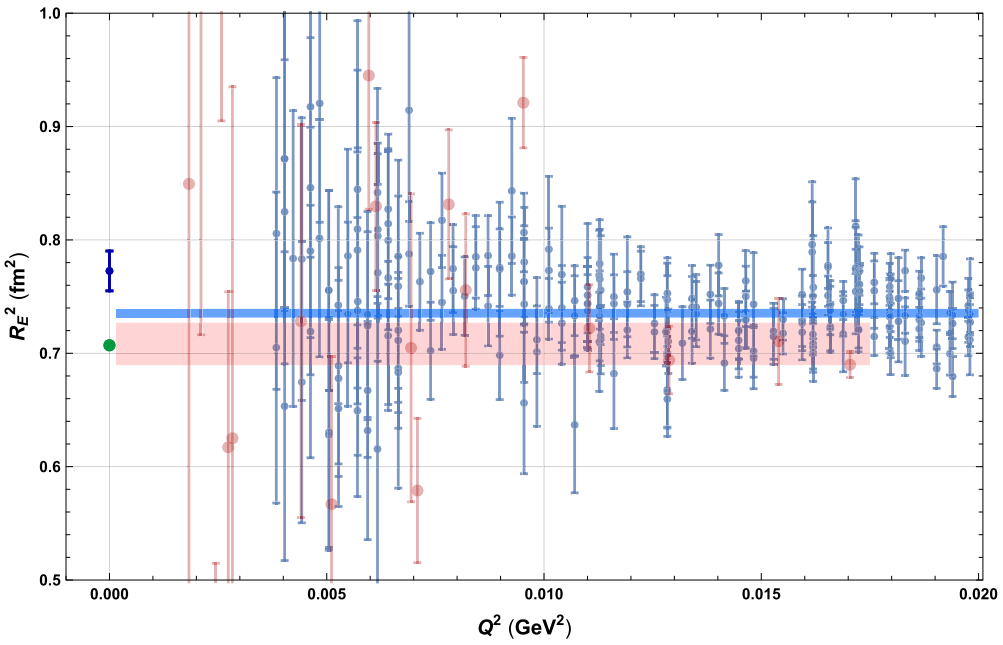

Fig. 2. The quantity $R_E^2(Q^2)$ defined in Eq. (6) for the proton, whose value at 0 represents the proton charge-radius squared. The dark-blue and green points at 0 indicate the *ep* and μH values, respectively. The light-blue data points represent the dataset of Bernauer et al. [3,4]. The light-red data points represent the ISR dataset of Mihovilović et al. [30]. The blue and red bands are the statistical averages of the corresponding datasets and are given numerically in Table 1.

value, we can average over any subset of these data. In the figure, the horizontal blue band is the statistical average of Bernauer's dataset, whereas the red band is the statistical average of the ISR dataset. These bands were obtained fitting a horizontal line through the respective datasets using the NonlinearModelFit routine of Mathematica [33]. The corresponding values are presented in, respectively, the 1st and 3rd row of Table 1.

This is how ideally the bound should be determined from the experimental data. However, the present experimental data have systematic uncertainties of which the most acute one is the unknown absolute normalization of the cross section. The Bernauer dataset, for example, is normalized in conjunction with the radius extraction. Thus, the data normalization and the extrapolation to $Q^2 = 0$ are done simultaneously in the same fit. Moreover, one can obtain an equally good representation of Bernauer's data by using a lower value of the radius and different normalization factors [34,35].

4.2. Overall normalization factor

To see how the normalization uncertainty affects the bound, let us suppose the experimental form factor has a small normalization error ϵ, such that $G_E^{(\mathrm{exp})} = (1+\epsilon)\, G_E$, with G_E having the usual interpretation. Then,

$$R_E^{2(\mathrm{exp})}(Q^2) = -\frac{6}{Q^2}\ln\left[(1+\epsilon)\, G_E(Q^2)\right] = R_E^2(Q^2) - \frac{6}{Q^2}\ln(1+\epsilon). \tag{18}$$

If ϵ is positive, this is not a problem — the lower bound is preserved: $R_E^{2(\mathrm{exp})}(Q^2) \le R_E^2$, for $\epsilon \ge 0$. In the case of $\epsilon < 0$, in a certain low-Q^2 region, the bound is violated:

$$R_E^{2(\mathrm{exp})}(Q^2) \not\le R_E^2, \quad \text{for } Q^2 < Q_0^2, \tag{19}$$

where Q_0 is the root of the following equation:

Table 1
The lower-bound value of the proton charge radius, R_E (in fm), from two experiments and three experimental data sets. The error corresponds to the 95% confidence interval (i.e., $\pm 2\sigma$), obtained from statistical errors alone. These results are represented by the bands in Figs. 2 and 3 with the corresponding color-coding. The value in the last row includes only the statistical error of experimental data, whereas the other two values include both statistical and systematic error, as described in the text.

Dataset		Average $\sqrt{R_E^2(Q^2)}$
Bernauer et al. [4]	$Q^2 < 0.02$ GeV^2	0.857 ± 0.010
	subset "1:3"	0.864 ± 0.016
Mihovilović et al. [30]	all data	0.842 ± 0.011

$$R_E^2(Q_0^2) - \frac{6}{Q_0^2}\ln(1+\epsilon) = R_E^2. \tag{20}$$

Assuming Q_0 is small, we can use the expanded form of $R_E^2(Q^2)$ in Eq. (11), to find:

$$Q_0^2 = \sqrt{\frac{-6\ln(1+\epsilon)}{\frac{1}{20}\langle r^4\rangle_E - \frac{1}{12}R_E^4}}. \tag{21}$$

For example, taking $\epsilon = -0.001$ and typical values of the radii [36], this equation gives $Q_0^2 \approx 0.01$ GeV^2. Therefore, one strategy for avoiding the possible normalization issue is to drop the data below a certain Q^2 value from the lower-bound evaluation.

Of course, this consideration only applies when all the data points of a given dataset have the same normalization factor. In reality, the experiment of Bernauer et al. [4] has a complicated normalization procedure, involving 31 normalization factors, and one can manage to obtain significant shifts of the data points by a different fit of these factors [34,35]. These shifts could then be considered as a systematic normalization uncertainty which is only partially attributed to an overall normalization.

Therefore, it is better to treat the overall-normalization uncertainty as a systematic error. In accounting for this highly-correlated error we use the method adopted by the PDG [37, Sec. 5.2]. Namely, the averaging of the dataset $A_i \pm \sigma_i \pm \Delta$, with Δ the

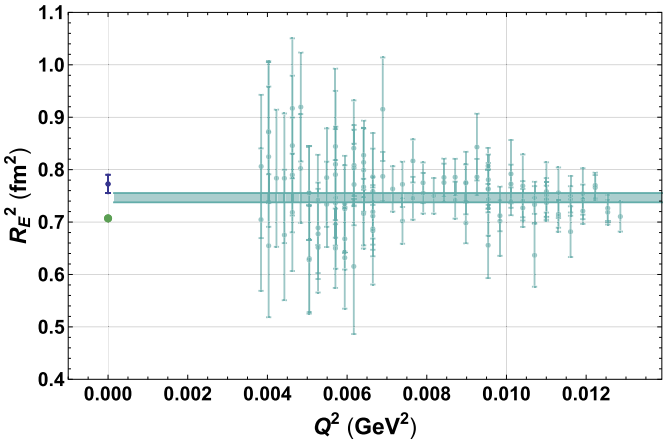

Fig. 3. The quantity $R_E^2(Q^2)$ of Eq. (6) for the normalization dataset "1:3" of Bernauer et al. [3]. The cyan band is the statistical average of the corresponding dataset and is given numerically in Table 1. The dark-blue and green points at 0 indicate the *ep* and μH values, respectively.

correlated systematic error, is equivalent to averaging the dataset $A_i \pm \sigma_i'$, where $\sigma_i' = (\sigma_i^2 + \Delta_i^2)^{1/2}$ is the redefined error with $\Delta_i^2 = \sigma_i^2 \Delta^2 \sum_j (1/\sigma_j^2)$. The systematic uncertainty of Bernauer's data on the reduced cross section, in the low-Q region, is of the order 10^{-3}. Taking the latter number for Δ, the error increases as $\sigma_i' \approx 4.5\sigma_i$, hence, the systematic error dominates in this dataset. The resulting average of the lower-bound function, including the systematic uncertainty, is given in the first row of Table 1. We have checked that the analogous account of the form-factor normalization uncertainty at the level of the $R^2(Q^2)$ quantity, rather than the cross section, results in a slightly smaller uncertainty on the bound. In either case, this error estimate is only indicative. In a more proper error evaluation one should use the covariance matrix established in the experimental analysis.

One can also identify subsets where the normalization is an overall factor. In the experimental data of Bernauer et al. these are, for example, normalization sets (see Supplement in [4]):

- 3 (spectrometer A, 180 MeV beam energy),
- 1:3 (spectrometer B, 180 MeV beam energy),
- 6:9 (spectrometer B, 315 MeV beam energy).

The most precise result is coming from the subset 1:3, because it is the largest in the relevant low-Q region. The resulting average for the subset 1:3 is shown in Fig. 3 and, including the above-mentioned systematic error, the second row of Table 1.

Both rows yield essentially the same lower bound: $R_E > 0.847$ fm at 95% confidence level (CL) for the full Bernauer's dataset vs. $R_E > 0.848$ fm for the subset 1:3. We chose to show only the former value in the summary plot of Fig. 1, cf. the blue band.

The average of the ISR data, shown in the last row of Table 1 (includes statistical errors only), yields a smaller lower bound: $R_E > 0.831$ fm at 95% CL, represented by the light-red band in Fig. 1.

5. Conclusion

An extraction of the proton charge radius from *ep* scattering requires an extrapolation to zero momentum transfer, which nowadays is entangled in the analysis of *ep* data. We aim here to get rid of the extrapolation issues in the interpretation of *ep* data. We show that the *ep* scattering may directly provide a lower bound on the proton charge radius, cf. Eq. (10) with Eq. (6). We emphasize that the lower-bound determination, unlike the extraction of the charge radius itself, does not involve any fitting of the Q^2-dependence with subsequent extrapolation to $Q^2 = 0$. Thus, the lower bound is a directly observable quantity (to the same extent as is the form factor), and is a more rigorous experimental outcome than the charge radius itself.

For illustrative purposes, we have made a tentative determination of the lower bound on the proton charge radius from the available data in the region of Q^2 below 0.02 GeV^2. The outcome for the two presently available experiments is given in Table 1. The lower bound resulting from Bernauer's dataset [$R_E > 0.847$ fm at 95% CL] appears to be in tension with the muonic-hydrogen results (see Fig. 1), albeit our uncertainty estimate is only indicative and should be taken with caution. The treatment of systematic errors, most notably the normalization uncertainty, is rather involved in this particular experiment and entangled with the radius extraction. For the bound determination one obviously needs the systematic errors of the cross section, to be determined independently of any radius extraction procedure.

Since the lower-bound function, defined in Eq. (6), is monotonically increasing with decreasing Q^2, the most stringent bound will be obtained from the lower Q^2 range, provided that the accuracy does not deteriorate with decreasing Q^2. Therefore, with the forthcoming results of the PRad experiment [38,39], one hopes to obtain a much better determination of the lower bound. The PRad data will reach down to 2×10^{-4} GeV^2 and include a simultaneous measurement of the Møller scattering. The latter will allow to further reduce the systematic uncertainties.

Acknowledgements

We are grateful to Jan Bernauer, Michael Distler, Miha Mihovilović, and Thomas Walcher for sharing their data with us and helpful communications; to Douglas Higinbotham for checking some of our results and an interesting discussion; to Patricia Bickert, Ashot Gasparyan, Vadim Lensky, and Stefan Scherer for useful remarks on the manuscript. This work was supported by the Swiss National Science Foundation and the Deutsche Forschungsgemeinschaft (DFG) through the Collaborative Research Center 1044 [The Low-Energy Frontier of the Standard Model].

References

[1] R. Hofstadter, R.W. McAllister, Electron scattering from the proton, Phys. Rev. 98 (1955) 217–218.
[2] R. Hofstadter, Nuclear and nucleon scattering of high-energy electrons, Annu. Rev. Nucl. Part. Sci. 7 (1957) 231–316.
[3] J. Bernauer, et al., High-precision determination of the electric and magnetic form factors of the proton, Phys. Rev. Lett. 105 (2010) 242001.
[4] J.C. Bernauer, M.O. Distler, J. Friedrich, T. Walcher, Electric and magnetic form factors of the proton, Phys. Rev. C 90 (2014) 015206.
[5] R. Pohl, et al., The size of the proton, Nature 466 (2010) 213–216.
[6] A. Antognini, et al., Proton structure from the measurement of 2S-2P transition frequencies of muonic hydrogen, Science 339 (2013) 417–420.
[7] P.J. Mohr, B.N. Taylor, D.B. Newell, Codata recommended values of the fundamental physical constants: 2010, Rev. Mod. Phys. 84 (2012) 1527–1605.
[8] P.J. Mohr, D.B. Newell, B.N. Taylor, CODATA recommended values of the fundamental physical constants: 2014, Rev. Mod. Phys. 88 (2016) 035009.
[9] A. Beyer, L. Maisenbacher, A. Matveev, R. Pohl, K. Khabarova, A. Grinin, T. Lamour, D.C. Yost, T.W. Hänsch, N. Kolachevsky, T. Udem, The Rydberg constant and proton size from atomic hydrogen, Science 358 (2017) 79–85.
[10] H. Fleurbaey, S. Galtier, S. Thomas, M. Bonnaud, L. Julien, F. Biraben, F. Nez, M. Abgrall, J. Guna, New measurement of the $1S - 3S$ transition frequency of hydrogen: contribution to the proton charge radius puzzle, Phys. Rev. Lett. 120 (2018) 183001.
[11] D. Borisyuk, Proton charge and magnetic rms radii from the elastic *ep* scattering data, Nucl. Phys. A 843 (2010) 59–67.
[12] R.J. Hill, G. Paz, Model independent extraction of the proton charge radius from electron scattering, Phys. Rev. D 82 (2010) 113005.
[13] X. Zhan, K. Allada, D. Armstrong, J. Arrington, et al., High precision measurement of the proton elastic form factor ratio $\mu_p G_E/G_M$ at low Q^2, Phys. Lett. B 705 (2011) 59–64.

[14] I. Sick, Problems with proton radii, Prog. Part. Nucl. Phys. 67 (2012) 473–478.
[15] K.M. Graczyk, C. Juszczak, Proton radius from Bayesian inference, Phys. Rev. C 90 (2014) 054334.
[16] J. Arrington, I. Sick, Evaluation of the proton charge radius from e-p scattering, J. Phys. Chem. Ref. Data 44 (2015) 031204.
[17] K. Griffioen, C. Carlson, S. Maddox, Consistency of electron scattering data with a small proton radius, Phys. Rev. C 93 (2016) 065207.
[18] G. Lee, J.R. Arrington, R.J. Hill, Extraction of the proton radius from electron-proton scattering data, Phys. Rev. D 92 (2015) 013013.
[19] D.W. Higinbotham, A.A. Kabir, V. Lin, D. Meekins, B. Norum, B. Sawatzky, Proton radius from electron scattering data, Phys. Rev. C 93 (2016) 055207.
[20] M. Horbatsch, E.A. Hessels, A. Pineda, Proton radius from electron-proton scattering and chiral perturbation theory, Phys. Rev. C 95 (2017) 035203.
[21] C. Adamuscin, S. Dubnicka, A. Dubnickova, New value of the proton charge root mean square radius, Prog. Part. Nucl. Phys. 67 (2012) 479–485.
[22] I.T. Lorenz, H.W. Hammer, U.-G. Meissner, The size of the proton – closing in on the radius puzzle, Eur. Phys. J. A 48 (2012) 151.
[23] I. Lorenz, U. Meißner, H. Hammer, Y. Dong, Theoretical constraints and systematic effects in the determination of the proton form factors, Phys. Rev. D 91 (2015) 014023.
[24] J.M. Alarcón, D. Higinbotham, C. Weiss, Z. Ye, Proton charge radius extraction from electron scattering data using dispersively improved chiral effective field theory, arXiv:1809.06373 [hep-ph], 2018.
[25] J.C. Bernauer, Avoiding common pitfalls and misconceptions in extractions of the proton radius, arXiv:1606.02159 [nucl-th], 2016.
[26] T.B. Hayward, K.A. Griffioen, Evaluation of low-Q^2 fits to *ep* and *ed* elastic scattering data, arXiv:1804.09150 [nucl-ex], 2018.
[27] X. Yan, D.W. Higinbotham, D. Dutta, H. Gao, A. Gasparian, M.A. Khandaker, N. Liyanage, E. Pasyuk, C. Peng, W. Xiong, Robust extraction of the proton charge radius from electron-proton scattering data, Phys. Rev. C 98 (2018) 025204.
[28] C.F. Perdrisat, V. Punjabi, M. Vanderhaeghen, Nucleon electromagnetic form factors, Prog. Part. Nucl. Phys. 59 (2007) 694–764.
[29] M. Hoferichter, B. Kubis, J. Ruiz de Elvira, H.W. Hammer, U.G. Meißner, On the $\pi\pi$ continuum in the nucleon form factors and the proton radius puzzle, Eur. Phys. J. A 52 (2016) 331.
[30] M. Mihovilović, et al., First measurement of proton's charge form factor at very low Q^2 with initial state radiation, Phys. Lett. B 771 (2017) 194–198.
[31] G.A. Miller, Transverse charge densities, Annu. Rev. Nucl. Part. Sci. 60 (2010) 1–25.
[32] R.N. Bracewell, The Fourier Transform and Its Applications, McGraw-Hill International Editions, 2000.
[33] W. R. Inc. Mathematica, Version 11.3, 2018, Champaign, IL.
[34] D.W. Higinbotham, Private communication (2018).
[35] D.W. Higinbotham, R.E. McClellan, How variation in analytic choices can affect normalization parameters and proton radius extractions from electron scattering data, arXiv:1902.08185 [physics.data-an], 2019.
[36] M.O. Distler, J.C. Bernauer, T. Walcher, The RMS charge radius of the proton and Zemach moments, Phys. Lett. B 696 (2011) 343–347.
[37] K.A. Olive, et al., Rev. Part. Phys., Chin. Phys. C 38 (2014) 090001.
[38] A. Gasparian, for the PRad at JLab Collaboration, The PRad experiment and the proton radius puzzle, EPJ Web Conf. 73 (2014) 07006.
[39] C. Peng, H. Gao, Proton charge radius (PRad) experiment at Jefferson lab, EPJ Web Conf. 113 (2016) 03007.